Normalised flux weakening control technique acting on the actual speed for automotive dual three-phase IPMSMs

A. Navarro-Temoche[1], E. Ibarra[1], I. Kortabarria[1], A. Sierra-González[2], I. Elosegui[3]
[1] University of the Basque Country (UPV/EHU)
[2] TECNALIA, Basque Research and Technology Alliance (BRTA)
[3] Tecnun, School of Engineering, University of Navarra
adrianorai.navarro@ehu.eus

Abstract

In this paper, a flux weakening control strategy based on a vector space decomposition (VSD) model is presented for asymmetrical dual three-phase interior permanent magnet synchronous machines (IPMSMs). This strategy incorporates a voltage magnitude feedback loop, which provides robustness by adding a variation to the actual speed when enters in flux weakening mode or deviations occur in the electrical parameters of the machine. Validity of the proposal is demonstrated by simulation results carried out over standardised driving cycles, taking into account parameter mismatches.

Keywords: Dual three-phase, IPMSM, EV, flux weakening

1 Introduction

Multi-phase machines are receiving a great attention as, compared to three-phase systems, they provide a reduced torque ripple, low harmonic content and an improved fault tolerance [1, 2]. The six-phase configuration is one of the most studied of the multi-phase architectures. Depending on the phase arrangement between the three-phase sets, they can be classified into symmetrical (shifted by 0 or $\pi/3$) [3,4] or asymmetrical (shifted by $\pi/6$) [5, 6]. With the asymmetrical configuration, the sixth harmonic torque pulsations produced by the two three-phase sets are in anti-phase and, therefore, they are cancelled [7].

Regarding the industrial integration of the dual three-phase permanent magnet synchronous machines (PMSMs), they have been successfully used in a variety of industry applications [8–11]. Among them, the automotive sector represents a highly demanding application, requiring operation for a very wide speed range and high torque [9–11].

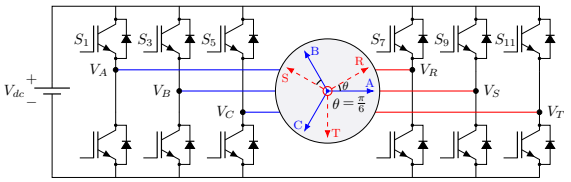

Figure 1: Asymmetrical dual three-phase PMSM drive system.

In [12], several topologies of multiphase converters are discussed. Fig. 1 shows the most common arrangement for a dual three-phase system, where two voltage source inverters (VSI) share a common DC-link and feed two three-phase sets with isolated neutral points.

To extend the operating speed range of an EV drive, which is constrained by the battery voltage, flux weakening (FW) needs to be applied. FW strategies can be classified as: *feedback*, where the ones regulating the voltage magnitude are the most common [13–15], *feed-forward*, where Look-up Tables (LUTs) or analytical calculations are used [16, 17], and *hybrid* [18, 19], which combine the merits of *feed-forward* and *feedback* solutions.

In this paper, a flux weakening control strategy based on a voltage magnitude feedback and considers a speed displacement as output, is proposed for dual-three phase IPMSMs. To do so, the actual speed is modified according to the voltage feedback and evaluated for maximising the voltage utilisation of the DC-link. Furthermore, to simplify the analysis, this algorithm is developed in a normalised system.

The rest of the paper is organised as follows: In section II, the mathematical model of a dual-three phase PMSMs is shortly introduced. Achievable operating regions are described in Section III. The flux weakening control based on a normalised system is developed in Section IV. Finally, simulation results are presented and discussed in Section IV, and conclusions are provided.

Table 1: Harmonic decomposition using VSD model.

Sub-space	Harmonics	h
$\alpha\beta$	Fund. and $(12k \pm 1) \Rightarrow k = 1, 2, 3, \ldots$	$1, 11, 13, \ldots$
XY	$(6k \pm 1) \Rightarrow k = 1, 3, 5, \ldots$	$5, 7, 17, 19, \ldots$
o_1o_2	$(3k) \Rightarrow k = 1, 3, 5, \ldots$	$3, 9, 15, 21, \ldots$

2 Mathematical modelling of dual three-phase PMSMs using VSD theory

To simplify the representation in phase variables, the six-dimensional machine system, according to the vector space decomposition (VSD) theory [20], can be used. This way, the machine is decomposed into three orthogonal sub-spaces, i.e. $\alpha\beta, XY$ and o_1o_2. By applying the transformation matrix T_6 of (1), harmonics are mapped to different sub-planes, as shown in Table 1.

$$\begin{bmatrix} F_\alpha & F_\beta & F_X & F_Y & F_{o_1} & F_{o_2} \end{bmatrix}^T = \\ = \mathbf{T}_6 . \begin{bmatrix} F_A & F_B & F_C & F_R & F_S & F_T \end{bmatrix}^T , \quad (1)$$

$$\mathbf{T}_6 = \frac{1}{3} \begin{bmatrix} 1 & \cos(4\theta_s) & \cos(8\theta_s) & \cos(\theta_s) & \cos(5\theta_s) & \cos(9\theta_s) \\ 0 & \sin(4\theta_s) & \sin(8\theta_s) & \sin(\theta_s) & \sin(5\theta_s) & \sin(9\theta_s) \\ 1 & \cos(8\theta_s) & \cos(4\theta_s) & \cos(5\theta_s) & \cos(\theta_s) & \cos(9\theta_s) \\ 0 & \sin(8\theta_s) & \sin(4\theta_s) & \sin(5\theta_s) & \sin(\theta_s) & \sin(9\theta_s) \\ 1 & 1 & 1 & 0 & 0 & 0 \\ 0 & 0 & 0 & 1 & 1 & 1 \end{bmatrix},$$

where $\theta_s = \pi/6$.

By applying the standard Park transformation, the variables in the $\alpha\beta$ sub-plane can be converted to the synchronous dq-frame for a dual three-phase system:

$$\begin{bmatrix} F_d \\ F_q \end{bmatrix} = \begin{bmatrix} \cos\theta & \sin\theta \\ -\sin\theta & \cos\theta \end{bmatrix} \begin{bmatrix} F_\alpha \\ F_\beta \end{bmatrix} = \mathbf{T_{dq}} F_{\alpha\beta}. \quad (2)$$

In addition, according to [21], the variables in the XY sub-plane can be converted to a new frame, designated as xy-frame, by applying the following transformation:

$$\begin{bmatrix} F_x \\ F_y \end{bmatrix} = \begin{bmatrix} -\cos\theta & \sin\theta \\ \sin\theta & \cos\theta \end{bmatrix} \begin{bmatrix} F_X \\ F_Y \end{bmatrix} = \mathbf{T_{xy}} F_{XY}, \quad (3)$$

where F can be V, I or ψ, which correspond to the voltage, current and flux, respectively. Then, the harmonics in the XY sub-plane are converted into $(6k)$th harmonics in the xy-frame.

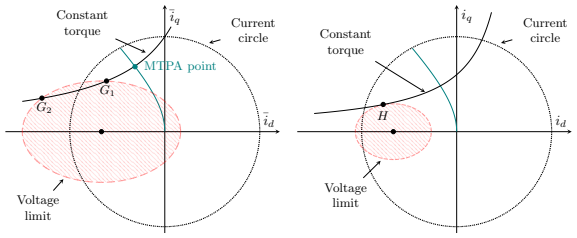

(a) FW. (b) MTPV.

Figure 2: Operating regions.

It is worth noting that the third sub-plane o_1o_2 cannot be exploited (i.e., open circuit), as the neutral point of each three-phase set is isolated and they are not connected between them. Hence, $I_{o_1} = I_{o_2} = 0$. Therefore, the voltage equations in the dq and xy-frames can be expressed as:

$$\begin{bmatrix} V_d \\ V_q \end{bmatrix} = \begin{bmatrix} R_s + L_d s & 0 \\ 0 & R_s + L_q s \end{bmatrix} \begin{bmatrix} I_d \\ I_q \end{bmatrix} + \omega_e \begin{bmatrix} -L_q I_q \\ L_d I_d + \lambda_m \end{bmatrix}, \\ \begin{bmatrix} V_x \\ V_y \end{bmatrix} = \begin{bmatrix} R_s + L_x s & 0 \\ 0 & R_s + L_y s \end{bmatrix} \begin{bmatrix} I_x \\ I_y \end{bmatrix} + \omega_e \begin{bmatrix} -L_y I_y \\ L_x I_x \end{bmatrix}, \quad (4)$$

where R_s is the stator resistance, λ_m is the permanent magnet flux linkage, and ω_e is the electrical speed of the machine. With respect to the inductances, L_d is the d-axis inductance, L_q is the q-axis inductance, and $L_{x,y} = L_{sl}$ are the inductances in the xy-frame where L_{sl} is the phase leakage inductance.

Finally, by assuming that the flux linkages in the dq-frame are linear functions, i.e., $\lambda_d = L_d I_d + \lambda_m$ and $\lambda_q = L_q I_q$, the electromagnetic torque is expressed as:

$$T_{em} = 3N_p(\lambda_m + (L_d - L_q)I_d)I_q. \quad (5)$$

where N_p is the number of pole-pairs. From (5), it is noted that the xy-frame does not contribute to the torque production.

3 Operating regions of dual three-phase IPMSMs

In this section, to simplify the analysis of the operating regions of the drive, a normalised system is utilised. The base values are collected in Table 2.

Table 2: Base values for IPMSMs [22].

Parameter	Value	Parameter	Value
Base electrical speed ω_b	$\omega_{e,N}$	Base current I_b	λ_m/L_d
Base voltage V_b	$\lambda_m\omega_{e,N}$	Base torque T_b	$3N_p\lambda_m^2/L_d$
Saliency ξ	L_q/L_d		

Regarding the achievable operation points, they are restricted by the current and voltage limits of the drive. Thus, the normalised maximum current (i_{max}) can be defined as [23]:

$$\sqrt{i_d^2 + i_q^2} = i_s \leq i_{max}, \tag{6}$$

where i_d and i_q are dq-frame current components, expressed in the normalised system, and i_s is the normalised modulus of the current vector. i_{max} can be higher or lower than 1, depending on whether the machine and inverter current limits are higher or lower than the base current I_b.

By normalising the dq-frame in (4), considering steady state operation and neglecting the voltage drop related to the stator resistance R_s, the normalised maximum voltage produced by the inverter without over-modulation (v_{max}) is expressed as [24]:

$$\begin{matrix} v_d = -i_q\Omega_e\xi, \\ v_q = \Omega_e(i_d+1), \end{matrix} \rightarrow (i_d+1)^2 + \xi^2 i_q^2 \leq \left(\frac{v_{max}}{\Omega_e}\right)^2, \tag{7}$$

where Ω_e is the normalised electrical speed and ξ is the saliency of the machine; v_d and v_q are the dq-frame voltage components expressed in the normalised system, and $v_{max} = V_{max}/V_b$ is the normalised maximum modulus of the voltage vector, where V_b is the base voltage. It should be noted that V_{max} depends on the used modulation strategy ($V_{dc}/\sqrt{3}$ for space vector modulation or PWM with third harmonic injection where, V_{dc} is the dc voltage bus).

On the other hand, by normalising (5), the electromagnetic torque (τ_{em}) is expressed as:

$$\tau_{em} = i_q[1 + (1-\xi)i_d], \tag{8}$$

were several i_d and i_q combinations that lead to the same torque value can be obtained. Thus, proper current trajectory calculations are fundamental if losses are to be reduced.

In accordance with (6) and (7), three operating regions can be distinguished for a synchronous machine: Maximum Torque per Ampere (MTPA), Flux Weakening (FW) and Maximum Torque per Voltage (MTPV), also known as deep flux weakening region.

Minimum copper losses and maximum torque per applied current modulus are guaranteed following the MTPA trajectory, which prevails at low speeds [25, 26]. An MTPA point is applicable provided that it is not located beyond the ellipse related to the voltage limit. Otherwise, flux weakening (FW) mode is reached and negative d-current is injected to guarantee minimum phase currents. The FW trajectory [Fig. 2(a)] is referred to the vectors intersecting the reference torque curve (G_1 and G_2 points).

Finally, the MTPV trajectory is defined as the curve where the maximum torque is reached with a minimum voltage [Point H, which intersects a maximum torque curve for a voltage limit is shown in Fig. 2(b)]. This trajectory minimises magnetic losses, which are prevalent at high speeds. In addition, MTPV region can be considered in the control provided that $i_{max} > 1$; otherwise, the MTPV curve cannot be exploited.

The purpose of the flux weakening control is to find a current pair that maximises the dc-link voltage utilisation and is within the voltage limit, but without exceeding the current limit.

4 Proposed Flux weakening control

In this paper, a FW control that considers all the aforementioned operation regions and determines the current reference trajectories in a normalised system is proposed.

As shown in Fig. 3, the FW algorithm is integrated in the Field Oriented Control (FOC). For a given reference torque, a dq-frame reference current pair (I_d^*, I_q^*) is generated. Furthermore, currents in the no-torque frame (i.e. xy) (I_x^*, I_y^*) are usually set to 0 for machines with sinusoidally distributed windings and, as the neutral points of the two three-phase sets are isolated and are not connected, currents in the o_1o_2 sub-space are zero. In addition, a PWM with 3rd harmonic injection, which pulses are sent to the two three-phase VSIs, is used.

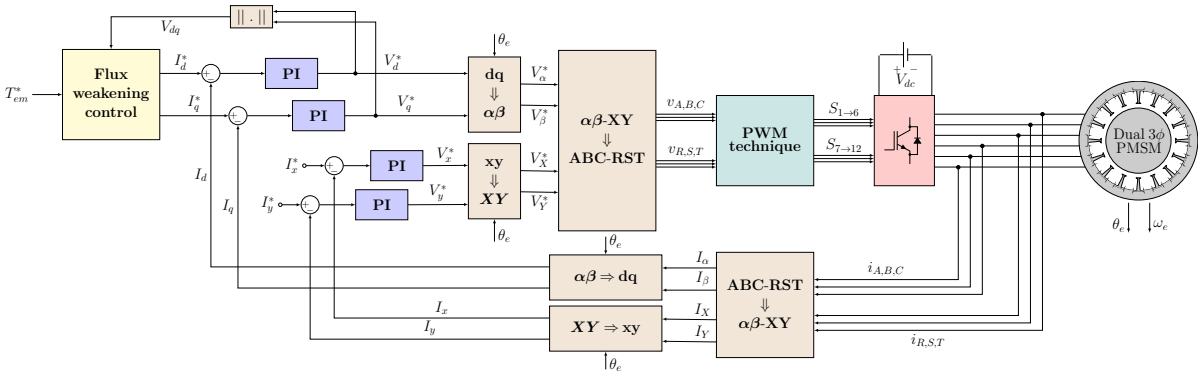

Figure 3: FOC structure for dual three-phase machines following the VSD representation.

Up to nominal speed, the current references I_d^* and I_q^* are generated to be referred to the MTPA curve, which guarantees minimum copper losses. To extend the operating speed range of this EV drive, for speeds beyond the nominal one, a flux weakening scheme is presented in Fig. 4. When the system enters in FW region, for a reference torque (τ_{em}^*), a normalised speed deviation ($\Delta\Omega$), coming from the voltage feedback (i.e., integral controller) is added to the actual speed (Ω_{ac}) to obtain an updated normalised speed (Ω_u), which is in charge of maintaining the stator voltage modulus inside the voltage limit.

The normalised maximum voltage available (v_{max}) is divided by Ω_u (v_{max}/Ω_u), which is used to calculate the current magnitudes, in the *dq*-frame, for all achievable operating regions.

For the MTPA, *d*-current calculation (i_d^{MTPA}) can be directly obtained from a given reference torque in a normalised system by analytically solving the following [19]:

$$\tau_{em}^* = \sqrt{\frac{i_d^{\text{MTPA}}}{1-\xi}[1+(1-\xi)i_d^{\text{MTPA}}]^3}. \tag{9}$$

Regarding the optimal currents in FW region, a fourth order polynomial can be obtained in terms of i_d if the optimisation problem, described in [25], is considered in a normalised system [19]. By using (v_{max}/Ω_u), this polynomial can be expressed as follows:

$$i_d^4 + A_n i_d^3 + B_n i_d^2 + C_n i_d + D_n = 0, \tag{10}$$

where,

$$A_n = \frac{2(2-\xi)}{1-\xi}\ ,\ B_n = \frac{\xi^2-6\xi+6}{(1-\xi)^2} - v_{max}^2/\Omega_u^2, \tag{11}$$

$$C_n = \frac{2}{(1-\xi)^2}\left[1+(1-\xi)(1-v_{max}^2/\Omega_u^2)\right], \tag{12}$$

$$D_n = \frac{1}{(1-\xi)^2}\left[1+\tau_{em}^2\xi^2 - v_{max}^2/\Omega_u^2\right]. \tag{13}$$

Analytical solution of (10) can be obtained by means of Ferrari's method, thoroughly detailed in [25]:

$$i_d^{\Omega_u} = \left(-\frac{A_n}{4} - \frac{\eta}{2} + \frac{\mu}{2}\right). \tag{14}$$

To this extent, in order to correctly operate in MTPA and FW regions at any speed, $i_d^{\Omega_u}$ is saturated to i_d^M as the upper bound, resulting in i_d'. From the latter, using the normalised torque equation of (8), i_q' can be obtained.

Furthermore, despite the fact that the MTPV region can be exploited provided that $i_{max} > 1$, an MTPV subsystem is added to the proposed algorithm for guaranteeing operating points within the voltage limit even when the voltage curve corresponding to Ω_u does not intersect with the torque curve. First, by normalising the MTPV trajectories defined in [25], the MTPV point is [19]:

$$i_d^{\text{MTPV}} = \frac{-\xi + \sqrt{\xi^2 + 8(v_{max}/\Omega_u)^2(1-\xi)^2}}{4(1-\xi)} - 1, \tag{15}$$

$$i_q^{\text{MTPV}} = \frac{1}{\xi}\sqrt{(v_{max}/\Omega_u)^2 - (i_d^{\text{MTPV}}+1)^2}. \tag{16}$$

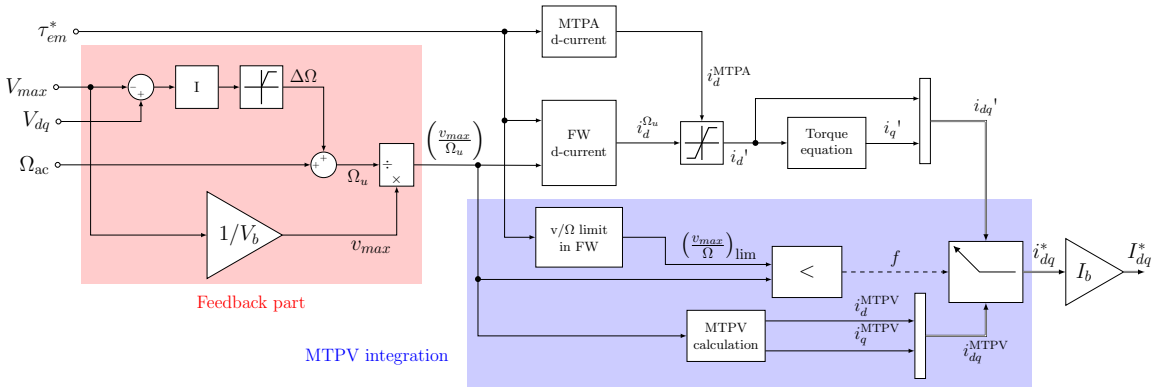

Figure 4: Block diagram of the proposed flux weakening strategy.

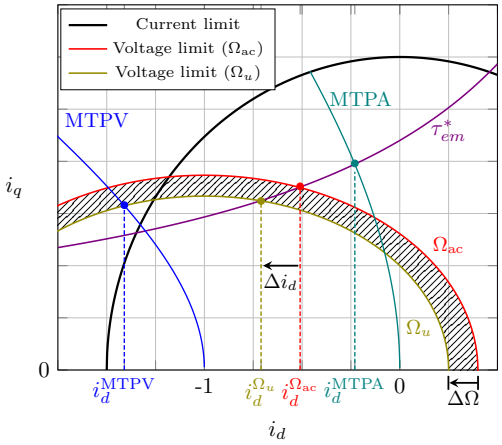

Figure 5: Operating principle of the proposed FW strategy.

Then, the maximum speed in FW region for the given torque $(v_{max}/\Omega)_{\text{lim}}$ (i.e the last voltage limit intersecting with the reference torque) must be calculated as, above this speed value, the machine operates within the MTPV curve. By equalising not only the q-current expressions from (7) and (8), but also their derivatives with respect to i_d (di_q/di_d), the quartic equation related to the last value of i_d in FW region is obtained:

$$(i_d + 1)(1 + (1 - \xi)i_d)^3 = \tau_{em}^2(1 - \xi)\xi^2. \quad (17)$$

Thus, the last value of i_q in FW is calculated from (8), and $(v_{max}/\Omega)_{\text{lim}}$ from (7). Once the latter is obtained, it is compared to v_{max}/Ω_u, such that if $(v_{max}/\Omega)_{\text{lim}} < v_{max}/\Omega_u$, the FW region is activated and the (i_d', i_q') point is applied. Otherwise, the $(i_d^{\text{MTPV}}, i_q^{\text{MTPV}})$ is set as reference. Once obtained the current references in the normalised system (i_{dq}^*), they have to be denormalised (I_{dq}^*) by multiplying them by the base current I_b.

Table 3: Parameters of the dual three-phase IPMSM drive.

Parameter	Value	Parameter	Value
Number of pole pairs N_p	19	Stator resistance R_s	61.43 [$m\Omega$]
d-axis inductance L_d	1.00 [mH]	q-axis inductance L_q	1.35 [mH]
PM flux linkage λ_m	0.038 [Wb]	DC bus nominal voltage V_{dc}	400 [V]
Maximum torque T_{max}	54 [N.m]	Maximum mech. speed ω_m	5000 [rpm]
Switching frequency	25 [kHz]	Simulation step	0.5 [μs]

To summarise, Fig. 5 exemplifies the performance of the algorithm. Once defined the voltage limits corresponding to Ω_{ac} and Ω_u, the d-axis current corresponding to the latter $(i_d^{\Omega_u})$ is calculated and saturated to i_d^{MTPA} as upper bound. This current will be shifted Δi_d from the d-current related to Ω_{ac} $(i_d^{\Omega_{\text{ac}}})$. Furthermore, whether the MTPV region is exploited or not, i_d^{MTPV} is considered and evaluated according to $(v_{max}/\Omega)_{\text{lim}}$.

5 Simulation results

A simulation model of an asymmetrical dual three-phase IPMSM drive, whose most relevant parameters are listed in Table 3, is implemented in the Matlab/Simulink environment together with the proposed controller.

The flux weakening strategy is tested under close-to-real driving conditions. Particularly, the torque and speed profiles are calculated for a given EV which is circulating under the Worldwide Harmonised Light vehicles Test Cycles (WLTC) Class

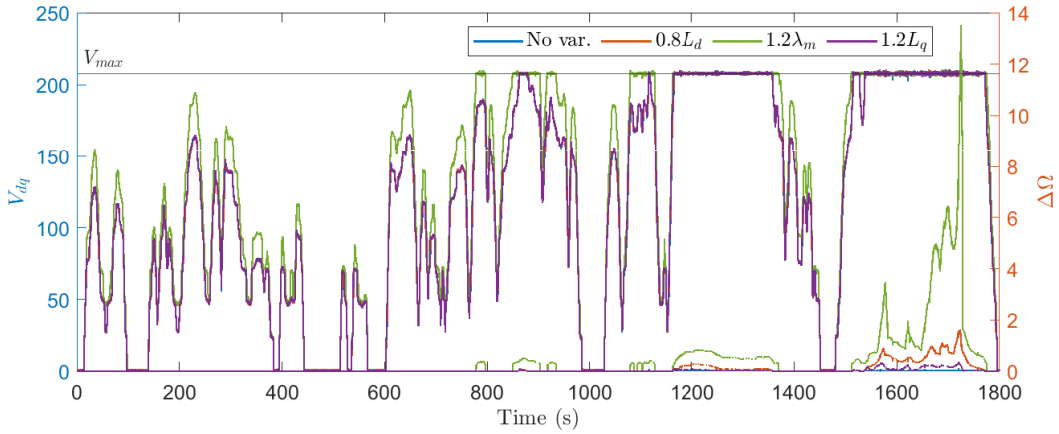

Figure 6: Voltage utilisation (V_{dq}) and voltage feedback output ($\Delta\Omega$) over the WLTC when parameter mismatches occur.

3. Considering the high computational burden of the model, i.e., the short discrete simulation step required to obtain accurate results without jitter (0.5 μs) and the long duration of the driving cycle, the model is loaded into an OPAL-RT OP4510 real-time digital platform (Intel Xeon E3 v5 CPU, 4 core, 8 MB cache, 3.5 GHz) and executed in the simulation mode (no real-time). Even though the flux weakening algorithm only enters when the vehicle operates at high speeds, simulations are exposed for the entire WLTC Class 3 driving cycle.

As parameter mismatch is one of the most important issues to be overtaken, the inductances L_{dq} and the flux linkage λ_m are modified in the machine to evaluate the robustness of the controller, specifically, the output of the voltage feedback loop. Although these parameters are simulated with a ± 20 % variation, results are only depicted for those that intensify the flux weakening action (i.e., $0.8L_d$, $1.2\lambda_m$, and $1.2L_q$). In addition, for this test, the integral gain K_i is set to 25.

On the one hand, the voltage utilisation and the output of the voltage feedback controller are plotted in Fig. 6. It is proved that the FW controller is capable of performing in all achievable regions as the updated speed (Ω_u) can easily enter in MTPV curve to maintain the operating point inside the voltage limit. It should be noted that updating the electrical speed is just a step of the FW controller to find the appropriate current-pair as the actual speed is not altered in the next stages of the FOC.

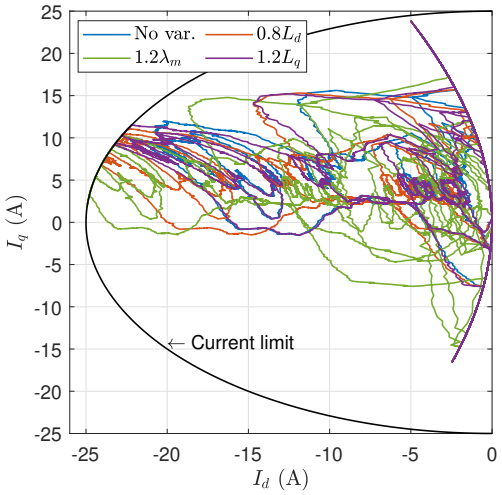

Figure 7: Reference dq-currents over the WLTC when parameter mismatches occur.

Finally, Fig. 7 shows the reference dq-currents set over the driving cycle. It is proved that the FW controller can operate taking into account the maximum current limit of the machine even when parameter mismatches occur. Furthermore, according to the results, the flux linkage mismatch causes the largest increment in the FW action.

6 Conclusions

In this paper, a normalised flux weakening control strategy, which acts on the actual speed, is pro-

posed. When a variation is provided by the voltage magnitude feedback loop, this is theoretically updated and evaluated in all achievable operating regions, such that the current reference maximises the dc-link utilisation. Although the proposed FW algorithm integrates quartic equations, they can be analytically calculated offline using the Ferrari's method, and replaced by LUTs. Thus, the computational burden will be substantially reduced.

Simulation results were carried out under a standardised driving cycle, particularly, the Worldwide Harmonised Light vehicles Test Cycles (WLTC) Class 3, with satisfactory performance in all achievable operating regions. Furthermore, under this test, the robustness of the FW controller is proved when parameter mismatches occur. In view of the above, the proposed technique is promising for experimental evaluation.

Acknowledgements

This work was supported in part by the Government of the Basque Country within the fund for research groups of the Basque University system IT1440-22 and by the MCIN/AEI/10.13039/501100011033 within the project PID2020-115126RB-I00.

References

[1] A. G. Yepes, O. Lopez, I. Gonzalez-Prieto, M. J. Duran, and J. Doval-Gandoy, "A comprehensive survey on fault tolerance in multiphase ac drives, part 1: General overview considering multiple fault types," *Machines*, vol. 10, no. 3, 2022.

[2] A. G. Yepes, I. Gonzalez-Prieto, O. Lopez, M. J. Duran, and J. Doval-Gandoy, "A comprehensive survey on fault tolerance in multiphase ac drives, part 2: Phase and switch open-circuit faults," *Machines*, vol. 10, no. 3, 2022.

[3] Z. Liang, D. Liang, P. Kou, and Q. Ze, "Modeling and bumpless switching control of symmetrical dual three-phase PMSM in two operating modes," *Electric Power Components and Systems*, vol. 48, no. 3, pp. 304–319, 2020.

[4] Z. Liang, D. Liang, P. Kou, and S. Jia, "Postfault control and harmonic current suppression for a symmetrical dual three-phase SPMSM drive under single-phase open-circuit fault," *IEEE Access*, vol. 8, pp. 67674–67686, 2020.

[5] Y. Luo and C. Liu, "A simplified model predictive control for a dual three-phase PMSM with reduced harmonic currents," *IEEE Transactions on Industrial Electronics*, vol. 65, no. 11, pp. 9079–9089, 2018.

[6] Z. Shen, D. Jiang, Z. Liu, D. Ye, and J. Li, "Common-mode voltage elimination for dual two-level inverter-fed asymmetrical six-phase PMSM," *IEEE Transactions on Power Electronics*, vol. 35, no. 4, pp. 3828–3840, 2020.

[7] K. Gopakumar, S. Sathiakumar, S. Biswas, and J. Vithayathil, "Modified current source inverter fed induction motor drive with reduced torque pulsations," *IEE Proceedings B Electric Power Applications*, vol. 131, pp. 159–164(5), 1984.

[8] Y. Xiao, C. Liu, and F. Yu, "An effective charging-torque elimination method for six-phase integrated on-board EV chargers," *IEEE Transactions on Power Electronics*, vol. 35, no. 3, pp. 2776–2786, 2020.

[9] A. Salem and M. Narimani, "A review on multiphase drives for automotive traction applications," *IEEE Transactions on Transportation Electrification*, vol. 5, no. 4, pp. 1329–1348, 2019.

[10] S. V. Nair, H. P., and K. Hatua, "Six-step operation of a symmetric dual three-phase PMSM with minimal circulating currents for extended speed range in electric vehicles," *IEEE Transactions on Industrial Electronics*, vol. 69, no. 8, pp. 7651–7662, 2022.

[11] S. V. Nair, K. Layek, and K. Hatua, "An unequal split dual three-phase pmsm with extended torque-speed characteristics for automotive application," *IEEE Transactions on Power Electronics*, vol. 37, no. 10, pp. 12437–12449, 2022.

[12] Z. Liu, Y. Li, and Z. Zheng, "A review of drive techniques for multiphase machines," *CES Transactions on Electrical Machines and Systems*, vol. 2, no. 2, pp. 243–251, 2018.

[13] W. Taha, D. F. Valencia, Z. Zhang, B. Nahid-Mobarakeh, and A. Emadi, "Adaptive flux weakening controller for dual three-phase PMSM drives in vector space decomposition," in *Proceedings of the Annual Conference of the IEEE Industrial Electronics Society (IECON)*, pp. 1–6, 2021.

[14] V. Manzolini, D. Da Rù, and S. Bolognani, "An effective flux weakening control of a SyRM drive including MTPV operation," *IEEE Transactions on Industry Applications*, vol. 55, no. 3, pp. 2700–2709, 2019.

[15] N. Bedetti, S. Calligaro, and R. Petrella, "Analytical design and autotuning of adaptive flux-weakening voltage regulation loop in IPMSM drives with accurate torque regulation," *IEEE Transactions on Industry Applications*, vol. 56, no. 1, pp. 301–313, 2020.

[16] S. Wang, J. Kang, M. Degano, A. Galassini, and C. Gerada, "An accurate wide-speed range control method of IPMSM considering resistive voltage drop and magnetic saturation," *IEEE Transactions on Industrial Electronics*, vol. 67, no. 4, pp. 2630–2641, 2020.

[17] H. Eldeeb, C. M. Hackl, L. Horlbeck, and J. Kullick, "A unified theory for optimal feed-forward torque control of anisotropic synchronous machines," *International Journal of Control*, vol. 91, no. 10, pp. 2273–2302, 2018.

[18] T.-S. Kwon, G.-Y. Choi, M.-S. Kwak, and S.-K. Sul, "Novel flux-weakening control of an IPMSM for quasi-six-step operation," *IEEE Transactions on Industry Applications*, vol. 44, no. 6, pp. 1722–1731, 2008.

[19] A. Navarro-Temoche, E. Ibarra, I. Kortabarria, A. Sierra-González, B. Prieto, and I. Elosegui, "Normalised hybrid flux weakening strategy for automotive asymmetrical dual three-phase IPMSMs," in *Proceedings of the Annual Conference of the IEEE Industrial Electronics Society (IECON)*, pp. 1–6, 2022.

[20] Y. Zhao and T. Lipo, "Space vector PWM control of dual three-phase induction machine using vector space decomposition," *IEEE Transactions on Industry Applications*, vol. 31, no. 5, pp. 1100–1109, 1995.

[21] Y. Hu, Z. Q. Zhu, and K. Liu, "Current control for dual three-phase permanent magnet synchronous motors accounting for current unbalance and harmonics," *IEEE Journal of Emerging and Selected Topics in Power Electronics*, vol. 2, pp. 272–284, 2014.

[22] C. Miguel-Espinar, D. Heredero-Peris, G. Gross, M. Llonch-Masachs, and D. Montesinos-Miracle, "Maximum torque per voltage flux-weakening strategy with speed limiter for PMSM drives," *IEEE Transactions on Industrial Electronics*, vol. 68, no. 10, pp. 9254–9264, 2021.

[23] S. Morimoto, M. Sanada, and Y. Takeda, "Wide-speed operation of interior permanent magnet synchronous motors with high-performance current regulator," *IEEE Transactions on Industry Applications*, vol. 30, no. 4, pp. 920–926, 1994.

[24] B.-H. Bae, N. Patel, S. Schulz, and S.-K. Sul, "New field weakening technique for high saliency interior permanent magnet motor," in *Proc. of the IAS Annual Meeting on Conference Record of the Industry Applications Conference*, vol. 2, pp. 898–905 vol.2, 2003.

[25] S.-Y. Jung, J. Hong, and K. Nam, "Current minimizing torque control of the IPMSM using Ferrari's method," *IEEE Transactions on Power Electronics*, vol. 28, no. 12, pp. 5603–5617, 2013.

[26] A. Dianov, F. Tinazzi, S. Calligaro, and S. Bolognani, "Review and classification of MTPA control algorithms for synchronous motors," *IEEE Transactions on Power Electronics*, vol. 37, no. 4, pp. 3990–4007, 2022.